Mutant *KRAS*-driven cancers depend on *PTPN11*/SHP2 phosphatase

Dietrich A. Ruess[1,5], Guus J. Heynen[2], Katrin J. Ciecielski[1], Jiaoyu Ai[1], Alexandra Berninger[1], Derya Kabacaoglu[1], Kivanc Görgülü[1], Zahra Dantes[1], Sonja M. Wörmann[1], Kalliope N. Diakopoulos[1], Angeliki F. Karpathaki[1], Marlena Kowalska[1], Ezgi Kaya-Aksoy[1], Liang Song[1], Eveline A. Zeeuw van der Laan[2], María P. López-Alberca[3], Marc Nazaré[3], Maximilian Reichert[1], Dieter Saur[1], Mert Erkan[4], Ulrich T. Hopt[5], Bruno Sainz Jr.[6], Walter Birchmeier[2], Roland M. Schmid[1], Marina Lesina[1] & Hana Algül[1]

[1] *Internal Medicine II, Klinikum rechts der Isar, Technische Universität München, München, Germany*
[2] *Cancer Research Program, Max Delbrück Center for Molecular Medicine (MDC) in the Helmholtz Society, Berlin, Germany*
[3] *Medicinal Chemistry, Leibniz-Forschungsinstitut für Molekulare Pharmakologie, Berlin, Germany*
[4] *Koç University School of Medicine, Istanbul, Turkey*
[5] *Department of Surgery, Medical Center – University of Freiburg, Faculty of Medicine, Freiburg, Germany*
[6] *Department of Biochemistry, Autónoma University of Madrid, School of Medicine, Instituto de Investigaciones Biomédicas "Alberto Sols", Madrid, Spain*

Corresponding Author:
Hana Algül, MD, MPH
Internal Medicine II
Klinikum rechts der Isar, Technische Universität München
Ismaninger Str. 22
81675 München, Germany.
Phone: +49 89 4140 5215**.**
Email: hana.alguel@mri.tum.de

The ubiquitously expressed non-receptor protein tyrosine phosphatase SHP2, encoded by *PTPN11*, is involved in signal transduction downstream of multiple growth factor, cytokine and integrin receptors[1]. Its requirement for complete RAS-MAPK activation and its role as a negative regulator of JAK-STAT signaling have established SHP2 as an essential player in oncogenic signaling pathways[1–7]. Recently, a novel potent allosteric SHP2-inhibitor was presented as a viable therapeutic option for RTK-driven cancers, but was shown to be ineffective in *KRAS* mutant tumor cell lines *in vitro*[8].

Here we report a central and indispensable role for SHP2 in oncogenic KRAS-driven tumors. Genetic deletion of *Ptpn11* profoundly inhibited tumor development in mutant *KRAS*-driven murine models of pancreatic ductal adenocarcinoma (PDAC) and non-small cell lung cancer (NSCLC). We provide evidence for a critical dependence of mutant KRAS on SHP2 during carcinogenesis. Deletion or inhibition of SHP2 in established tumors delayed tumor progression but was not sufficient to achieve tumor regression. However, SHP2 was necessary for resistance mechanisms upon blockade of MEK. Synergy was observed when both SHP2 and MEK were targeted, resulting in sustained tumor growth control in murine and human patient-derived organoids and xenograft models of PDAC and NSCLC. Our data suggest clinical utility of dual SHP2/MEK inhibition as a targeted therapy approach for *KRAS* mutant cancers.

RAS genes constitute the most frequently mutated oncogene family in human cancers[9]. While *KRAS* mutations are virtually universal in PDAC, they occur in up to 30% of NSCLC[9,10]. Recently, genome-wide association analysis and functional characterization identified the long intergenic noncoding RNA LINC00673 as a potential tumor suppressor that acts through regulation of PRPF19-mediated ubiquitination and degradation of SHP2 in PDAC. The germline G>A variation at rs11655237 impairs this effect of LINC00673 and confers susceptibility to tumorigenesis[11], implying a proto-oncogenic role for SHP2. In addition, SHP2 promotes RAS-RAF-MEK-ERK-signaling in NSCLC with EGFR-activating mutations[12,13], but evidence for its relevance in *KRAS* mutant NSCLC is lacking.

Oncogenomic database analysis together with protein expression profiling in several human PDAC and NSCLC tissues and cell lines revealed the epithelial presence of SHP2 (**Supplementary Fig. 1a-e**). As a sign of recruitment and activation, its Y542-phosphorylation[14–16] was detected in a heterogeneous pattern in the majority of samples analyzed (**Supplementary Fig. 1b-d**). Transcriptional levels of *PTPN11* had no clear association with overall survival in TCGA RNAseq PDAC and NSCLC (*KRAS* mutant subgroup) datasets (**Supplementary Fig. 1f,g**). These results suggest that SHP2 activation rather than expression levels determine its action in PDAC and NSCLC.

To genetically dissect the contribution of SHP2 in PDAC and NSCLC tumorigenesis, we utilized oncogenic KRAS-driven murine cancer models, which allow for tissue specific expression of $KRAS^{G12D}$ and the initiation of tumors in the pancreas or lung[17,18]. In both PDAC and NSCLC models SHP2 expression was observed during the entire process of tumor development **(Supplementary Fig. 2a-e)**. Pancreas-specific biallelic deletion of *Ptpn11* in $KRAS^{G12D}$ mice (termed: *Kras*), but not monoallelic deletion (data not shown), led to profound inhibition of PanIN (pancreatic intraepithelial neoplasia) development **(Fig. 1a,b and Supplementary Fig. 3a)**, pancreatic enlargement **(Supplementary Fig. 3b)** and desmoplasia **(Fig. 1a and Supplementary Fig. 3c)**. PDAC formation was almost completely blocked and survival was dramatically prolonged when *Ptpn11* was deleted (**Fig. 1c and Supplementary Fig. 3d**). Likewise, inflammation-triggered acceleration of pancreatic carcinogenesis by caerulein was inhibited in the absence of SHP2 (**Supplementary Fig.3e-h**). In an *ex vivo* acinar to ductal metaplasia (ADM) assay[19], genetic deletion and pharmacologic inhibition revealed a requirement of SHP2 and its phosphatase activity for efficient acinar trans-differentiation (**Supplementary Fig. 3i,j)**. Next, we took advantage of the more aggressive and tumor-prone PDAC mouse models with loss of *Ink4a/Arf*[20] or mono-/biallelic deletion of *Trp53*[21]. Strikingly, even in these backgrounds *Ptpn11* deficiency potently blocked PanIN progression and PDAC development, translating into significant and extended tumor free survival (**Fig. 1d,e and Supplementary Fig. 4a**). Only few macroscopic tumors were detected in *Kras;Trp53*$^{+/-}$*;Ptpn11*$^{-/-}$ or *Kras;Trp53*$^{-/-}$*;Ptpn11*$^{-/-}$ mice and none in *Kras;Ink4a/Arf*$^{-/-}$*;Ptpn11*$^{-/-}$ mice (**Supplementary Fig. 4b-d**). Comparable observations were made in a $KRAS^{G12D}$-driven model of NSCLC. The pulmonary 'atypical adenomatous hyperplasia – adenoma – adenocarcinoma' progression sequence was significantly delayed in the absence of *Ptpn11* (**Supplementary Fig. 5a-c,f**). Even in the more rapid *Kras;Trp53*$^{-/-}$ context, loss of *Ptpn11* resulted in a substantial deceleration of NSCLC-disease dynamics and reduced tumor burden, translating into considerably prolonged survival (**Fig. 1f and Supplementary Fig. 5d,e,g,h**). Of note, unlike in the PDAC models, a substantial fraction of tumors that emerged in the NSCLC models demonstrated escape from *Ptpn11* deletion (**Supplementary Fig. 5i**). Taken together, these *in vivo* data indicate a central and indispensable role for SHP2 in carcinogenesis of oncogenic KRAS-driven epithelial tumors of the pancreas and lung.

Formation of preneoplastic lesions and progression to carcinoma in these $KRAS^{G12D}$-driven models correlates with enhancement of RAF/MEK/ERK signaling[22,23]. However, phosphorylation of ERK in early transforming *Kras* pancreata or lungs was greatly diminished in *Kras;Ptpn11*$^{-/-}$ mice (**Fig. 2a and Supplementary Figs. 5j,k and 6a**). Additionally, the direct and indirect oncogenic RAS-effector PI3K/AKT- and STAT3-pathways were activated in transforming *Kras,* but not in *Kras;Ptpn11*$^{-/-}$ pancreata (**Fig. 2a**). Considerably decreased

levels of RBD-bound pan-RAS as well as RBD-bound $KRAS^{G12D}$ in tissue lysates of *Kras;Ptpn11*$^{-/-}$ pancreata (**Fig. 2b**) suggested severe RAS signaling defects upon *Ptpn11* deletion. To gain a more comprehensive insight into the impact of abrogated *Ptpn11* in $KRAS^{G12D}$ expressing pancreata we performed transcriptomics on pancreatic tissue samples from 9 week old mice. Gene set enrichment analysis revealed a remarkably skewed pattern of significantly enriched gene sets in favor of *Kras*, compared to *Kras;Ptpn11*$^{-/-}$ samples (**Fig. 2c and Supplementary Fig. 6b,c**). Enriched gene sets in *Kras* tissue included established oncogenic facets such as increased transcriptional activity, transdifferentiation, cell stress and altered metabolism, as well as inflammation, desmoplasia and (re-) activation of embryonic signaling cascades (**Supplementary Fig. 6b-f**). More importantly, a clear loss of a KRAS signaling signature was evident in *Kras;Ptpn11*$^{-/-}$ samples (**Fig. 2d**). Consequently, and consistent with the findings in **Fig. 2a,** signatures related to pathways that are known to be directly or indirectly linked to oncogenic KRAS*,* such as MEK, AKT and IL6-JAK-STAT3 signaling were lost with *Ptpn11* deletion (**Supplementary Fig. 6h**). In addition, *Kras* samples demonstrated enrichment of signatures of multiple growth factors, RTKs and immediate signal transducers upstream of RAS, suggesting a SHP2-dependent positive feedback loop for amplification of RAS activity above an oncogenic threshold[24] (**Supplementary Fig. 6g**). To further demonstrate the dependency of oncogenic KRAS on SHP2 in pancreatic carcinogenesis we first bred *Ptpn11* mice with $MAP2K1^{DD}$ or $PIK3CA^{H1047R}$ mice[25,26]. These crossings revealed that *Ptpn11* is redundant in the presence of constitutively active mutant MEK1 or PI3K (**Fig. 2e**) and SHP2 thus functions upstream, at the level of KRAS. Given the pleiotropic regulatory effects of SHP2 on signaling pathways, and its inhibitory role in the STAT3 pathway in particular[6], we further utilized a previously published $KRAS^{G12D}$ mouse model lacking the negative feedback STAT3-regulator SOCS3 specifically in the pancreas *(Kras;Socs3*$^{-/-}$*)*[27]. Loss of *Ptpn11* in this model did not further aggravate, but rescued the aggressive STAT3-dependent phenotype of PDAC development (**Supplementary Fig. 7a-c**), suggesting a requirement of SHP2 for inflammatory, paracrine oncogenic circuits, elicited by $KRAS^{G12D}$ and mediated by STAT3[27]. These genetic *in vivo* data demonstrate a dominant upstream role for SHP2 in regulating both adequate activity and oncogenic potency of $KRAS^{G12D}$ in pancreatic carcinogenesis.

To examine the contribution of SHP2 in tumor maintenance we utilized a dual recombinase approach[28]: Mice with pancreas-specific Flippase-mediated recombination (*Pdx-Flpo*) of *FSF-Kras*$^{G12D/+}$ and *Trp53*$^{frt/frt}$ alleles were monitored with MRI for tumor occurrence. Upon tumor detection, deletion of *Ptpn11* was achieved by a tamoxifen-inducible Cre-recombinase, expressed exclusively in the Flpo-recombined epithelial PDAC-compartment (*FSF-CreRT*). Subsequently, tumor dynamics were evaluated weekly with MRI (**Fig. 3a**). These experiments revealed that deletion of *Ptpn11* in established murine PDAC epithelia was not

sufficient to achieve tumor regression or prolongation of survival, but led to slower tumor growth and reduced pan-RAS- and $KRAS^{G12D}$-activity levels *in vivo* and *in vitro*; tumor morphology was unchanged (**Fig. 3b-e and Supplementary Fig. 8a-h)**.

In line with this finding, CRISPR/Cas9 mediated knockout of *PTPN11* in two *KRAS* mutant human PDAC cell lines (YAPC: $KRAS^{G12V}$; PANC-1: $KRAS^{G12D}$) resulted in reduced *in vitro* proliferation (with serum-rich 10% FBS conditions), delayed tumor growth in an *in vivo* xenograft-setting and diminished RBD-bound KRAS levels **(Supplementary Fig. 8i-l)**.

Aiming to identify pharmacologic vulnerabilities conferred by loss of SHP2 we performed a focused drug screen with *PTPN11* knockout cells using PDAC and NSCLC relevant chemotherapeutics (gemcitabine, oxaliplatin, paclitaxel) and selected small molecules targeting RAS-downstream effector kinases (PI3K, MEK). These experiments revealed that *PTPN11* knockout cells were uniquely susceptible to MEK inhibitors **(Fig. 3f and Supplementary Fig. 9a,b)**. Intrinsic and acquired resistance to MEK inhibition is a common phenomenon that has been attributed to activation of RTK signaling in *KRAS* mutant and *BRAF* mutant contexts[29–34]. Thus, MEK inhibitors have failed to enter into the clinic as a single adjunct to conventional chemotherapy in PDAC and NSCLC[35,36]. The *KRAS* mutant human PDAC cell lines YAPC, PANC-1 and DAN-G cells are relatively resistant to MEK inhibition, whereas CAPAN-2 is sensitive (**Supplementary Fig. 10a**). After prolonged treatment with selumetinib, phosphorylation of ERK increased steadily over time reaching near untreated control levels in YAPC, PANC-1 and DAN-G cells, while CAPAN-2 cells were incapable of reactivating ERK (**Supplementary Fig. 10b**). In parallel, we observed phosphorylation of multiple RTKs, strong Y542-phosphorylation and increased phosphatase activity of SHP2 upon treatment with selumetinib (**Fig. 3g and Supplementary Fig. 10b-f**), suggesting that SHP2 transmits a RTK-mediated feedback loop, conferring resistance to MEK inhibitors. Indeed, YAPC and PANC-1 *PTPN11* knockout cells were incapable of reactivating MAPK signaling in the presence of selumetinib (**Fig. 3h and Supplementary Fig. 10g).** Reconstitution of wild-type SHP2 or phosphatase-dead $SHP2^{C459S}$ in the *PTPN11* knockout cells demonstrated the requirement of SHP2 phosphatase activity for restoration of MAPK signaling and proliferative capacity in response to selumetinib (**Supplementary Fig. 11a,b**). Since these results provided a strong rationale for a dual SHP2/MEK inhibition, we targeted SHP2 in co-inhibition assays with two different compounds which have been previously characterized in detail, namely the catalytic-site inhibitor GS493[37] or the recently reported compound SHP099[8,38], which allosterically stabilizes SHP2 in its closed auto-inhibited conformation[38]. Their different modes of action were confirmed in a *PTPN11* knockout PANC-1 cell line, reconstituted with the $SHP2^{E76A}$ mutation perturbing autoinhibition and thus rendering the allosteric inhibitor ineffective **(Supplementary Figure 11c)**. Both compounds phenocopied the effect seen in *PTPN11* knockout cells and demonstrated

remarkable synergism with the MEK inhibitors selumetinib and trametinib in multiple murine and human PDAC and NSCLC cell lines. In addition, GS493 and SHP099 showed synergistic potential in combination with PI3K inhibitors but not with conventional chemotherapeutics (**Fig. 3i and Supplementary Figs. 11d-h and 12a,b**). The panel in **Supplementary Fig. 13a,b** demonstrates that synergism of combined SHP2/MEK inhibition is not restricted to *KRAS* mutant, but also evident in various *KRAS* wild-type tumor cell lines.

To test the translational relevance of our findings we set up three levels of experiments. We first treated endogenous PDAC-bearing *Kras;Trp53*$^{-/-}$ mice with GS493, with trametinib, or in combination. Similar to the results with human cell line xenotransplants **(Supplementary Fig. 8l)** GS493 alone only modestly inhibited tumor progression. As reported for selumetinib[39], trametinib, which possesses superior pharmacodynamics compared to other MEKi[40], achieved initial pancreatic volume reduction, but eventually resistant tumors emerged. Co-treatment with trametinib + GS493, however, impeded resistance-dynamics and achieved sustained tumor growth inhibition (**Fig. 4a,b and Supplementary Fig. 14a-d**). Similar potent effects were observed with NSCLC-bearing *Kras;Trp53*$^{-/-}$ AdCre mice, where marked total lesion volume regression was obtained with dual SHP2/MEK inhibition (**Fig. 4c and Supplementary Fig. 15a-e**). In line with previous observations, co-inhibition resulted in sustained reduction of ERK phosphorylation and decreased tumor proliferation in both models (**Supplementary Figs. 14e,f and 15f,g**). Secondly, primary patient-derived *ex vivo* *KRAS* mutant PDAC organoids exhibited reduced IC50 values for trametinib upon addition of SHP099 (**Fig. 4d and Supplementary Fig. 16**). And lastly, patient derived KRAS^{G12D} tumor tissue xenografts demonstrated *in vivo* susceptibility to combined SHP2/MEK inhibition (**Fig. 4e,f and Supplementary Fig. 17a-d**). Illustrated with PDAC ID_02, trametinib induced enhancement of pan-RAS- and KRAS^{G12D}-activity as well as the PI3K-pathway; however, in the dual treatment arm these effects were constrained, culminating in significantly reduced proliferation, elevated Cleaved Caspase-3 levels, and complete growth inhibition. Of note, SHP2 inhibition did not have detrimental effects on STAT3 phosphorylation. Taken together, these results demonstrate a potent synergistic effect of combined SHP2 and MEK inhibition in *KRAS* mutant carcinomas.

While SHP2 has been considered to be dispensable for mutated oncogenic KRAS function[8], using mouse and human pancreatic and lung cancer models combined with genetic and pharmacological inhibition approaches, our data indicate that oncogenic KRAS-activity depends on SHP2 for its intensification and for downstream signaling during carcinogenesis. In established tumors, loss or inhibition of SHP2 decelerates tumor progression and more importantly, SHP2 is required to reestablish RAS signaling when downstream RAS effectors (e.g. MEK) are inhibited. Since RTK-mediated (context dependent: ERBB family[31], ERBB family/PDGFRα/AXL[32], FGFR1[34]) resistance to MEK inhibition is a frequent and clinically

relevant problem in PDAC and *KRAS* mutant NSCLC, a therapeutic strategy comprising inhibitors of MEK with novel agents targeting SHP2 could putatively overcome this clinical barrier. As an integrator of RTK-RAS signaling downstream of almost all RTKs, our findings, together with those from the accompanying manuscript by Mainardi S. et al.[41], reveal that SHP2 may hold promise as a therapeutic target not only in RTK-driven, but also in *KRAS* mutant tumors.

ACKNOWLEDGEMENTS

We thank Gen-Sheng Feng (Department of Pathology, School of Medicine, and Molecular Biology, Division of Biological Sciences, University of California, San Diego, La Jolla, CA, USA) for sharing the *Ptpn11*^{fl} allele. Rickmer F. Braren and Dimitrios C. Karampinos (both Institute of Radiology, Klinikum rechts der Isar, Technische Universität München, Germany) provided the infrastructure and Aayush Gupta helped with the setup for MR imaging studies. This work was supported by grants from *Deutsche Forschungsgemeinschaft* (DFG AL1174/5-1 to H.A. and LE3222/1-1 to M.L.), *Deutsche Krebshilfe* (#111646 and #111464 to H.A.; Max Eder Program #111273, to M.R.), the *Wilhelm Sander Stiftung* (2014.052.1 to H.A.) and from Fundación Asociación Española Contra el Cáncer (to B.S.).

AUTHOR CONTRIBUTIONS

Conceptualization and study design: D.A.R., H.A. and G.J.H. Animal experiments: D.A.R. Histologic scoring, immunohistochemistry and immunofluorescence: D.A.R., A.B., D.K. and M.L. Immunoblotting: D.A.R., G.J.H., K.J.C., J.A., A.B. and E.A.Z.v.d.L. *In vitro* experiments with human PDAC cell lines including CRISPR/Cas9 knockout and reconstitution experiments: G.J.H. and E.A.Z.v.d.L. *In vitro* drug screening: K.J.C. and D.A.R. Oncogenomic database and gene set enrichment analyses: D.A.R. Maintenance of mouse colonies and genotyping: D.A.R., K.J.C., J.A., D.K., K.G., K.N.D., S.M.W., M.L., A.F.K., A.B., M.K., E.K.-A. and L.S. Synthesis of GS493 and SHP099: M.P.L.-A., M.N. and W.B. *Ex vivo* organoid assay: K.J.C., Z.D., D.A.R. and M.R. Generation of mutant mouse alleles: D.S. Establishment of PDAC-PDX: M.E. and B.S. Data analysis: D.A.R., G.J.H., K.J.C and H.A. Visualization: D.A.R., G.J.H. and K.J.C. Writing original draft: D.A.R. and H.A., with input from B.S. and G.J.H. Supervision: H.A. Providing funding: H.A., M.L., M.R., U.T.H., R.M.S, B.S. and W.B. All authors critically revised and approved the manuscript.

COMPETING FINANCIAL INTERESTS

None.

REFERENCES

1. Neel, B. G., Gu, H. & Pao, L. The 'Shp'ing news: SH2 domain-containing tyrosine phosphatases in cell signaling. *Trends Biochem. Sci.* **28,** 284–293 (2003).
2. Xu, D. & Qu, C.-K. Protein tyrosine phosphatases in the JAK/STAT pathway. *Front. Biosci. J. Virtual Libr.* **13,** 4925–4932 (2008).
3. Chan, G., Kalaitzidis, D. & Neel, B. G. The tyrosine phosphatase Shp2 (PTPN11) in cancer. *Cancer Metastasis Rev.* **27,** 179–192 (2008).
4. Matozaki, T., Murata, Y., Saito, Y., Okazawa, H. & Ohnishi, H. Protein tyrosine phosphatase SHP-2: A proto-oncogene product that promotes Ras activation. *Cancer Sci.* **100,** 1786–1793 (2009).
5. Chan, R. J. & Feng, G.-S. PTPN11 is the first identified proto-oncogene that encodes a tyrosine phosphatase. *Blood* **109,** 862–867 (2006).
6. Bard-Chapeau, E. A. *et al.* Ptpn11/Shp2 acts as a tumor suppressor in hepatocellular carcinogenesis. *Cancer Cell* **19,** 629–639 (2011).
7. Grossmann, K. S., Rosário, M., Birchmeier, C. & Birchmeier, W. Chapter 2 - The Tyrosine Phosphatase Shp2 in Development and Cancer. in *Advances in Cancer Research* (ed. Klein, G. F. V. W. and G.) **106,** 53–89 (Academic Press, 2010).
8. Chen, Y.-N. P. *et al.* Allosteric inhibition of SHP2 phosphatase inhibits cancers driven by receptor tyrosine kinases. *Nature* **535,** 148–152 (2016).
9. Cox, A. D., Fesik, S. W., Kimmelman, A. C., Luo, J. & Der, C. J. Drugging the undruggable RAS: Mission possible? *Nat. Rev. Drug Discov.* **13,** 828–851 (2014).
10. Almoguera, C. *et al.* Most human carcinomas of the exocrine pancreas contain mutant c-K-ras genes. *Cell* **53,** 549–554 (1988).
11. Zheng, J. *et al.* Pancreatic cancer risk variant in LINC00673 creates a miR-1231 binding site and interferes with PTPN11 degradation. *Nat. Genet.* **48,** 747–757 (2016).
12. Schneeberger, V. E. *et al.* Inhibition of Shp2 suppresses mutant EGFR-induced lung tumors in transgenic mouse model of lung adenocarcinoma. *Oncotarget* (2015).
13. Xu, J., Zeng, L.-F., Shen, W., Turchi, J. J. & Zhang, Z.-Y. Targeting SHP2 for EGFR inhibitor resistant non-small cell lung carcinoma. *Biochem. Biophys. Res. Commun.* **439,** 586–590 (2013).
14. Vogel, W., Lammers, R., Huang, J. & Ullrich, A. Activation of a phosphotyrosine phosphatase by tyrosine phosphorylation. *Science* **259,** 1611–1614 (1993).
15. Feng, G. S., Hui, C. C. & Pawson, T. SH2-containing phosphotyrosine phosphatase as a target of protein-tyrosine kinases. *Science* **259,** 1607–1611 (1993).
16. Lu, W., Shen, K. & Cole, P. A. Chemical dissection of the effects of tyrosine phosphorylation of SHP-2. *Biochemistry (Mosc.)* **42,** 5461–5468 (2003).
17. Hingorani, S. R. *et al.* Preinvasive and invasive ductal pancreatic cancer and its early detection in the mouse. *Cancer Cell* **4,** 437–450 (2003).
18. Jackson, E. L. *et al.* Analysis of lung tumor initiation and progression using conditional expression of oncogenic K-ras. *Genes Dev.* **15,** 3243–3248 (2001).
19. Means, A. L. *et al.* Pancreatic epithelial plasticity mediated by acinar cell transdifferentiation and generation of nestin-positive intermediates. *Dev. Camb. Engl.* **132,** 3767–3776 (2005).
20. Aguirre, A. J. *et al.* Activated Kras and Ink4a/Arf deficiency cooperate to produce metastatic pancreatic ductal adenocarcinoma. *Genes Dev.* **17,** 3112–3126 (2003).
21. Bardeesy, N. *et al.* Both p16(Ink4a) and the p19(Arf)-p53 pathway constrain progression of pancreatic adenocarcinoma in the mouse. *Proc. Natl. Acad. Sci. U. S. A.* **103,** 5947–5952 (2006).
22. Collisson, E. A. *et al.* A central role for RAF→MEK→ERK signaling in the genesis of pancreatic ductal adenocarcinoma. *Cancer Discov.* **2,** 685–693 (2012).
23. Blasco, R. B. *et al.* c-Raf, but not B-Raf, is essential for development of K-Ras oncogene-driven non-small cell lung carcinoma. *Cancer Cell* **19,** 652–663 (2011).
24. di Magliano, M. P. & Logsdon, C. D. Roles for KRAS in pancreatic tumor development and progression. *Gastroenterology* **144,** 1220–1229 (2013).
25. Srinivasan, L. *et al.* PI3 kinase signals BCR-dependent mature B cell survival. *Cell*

139, 573–586 (2009).
26. Eser, S. *et al.* Selective requirement of PI3K/PDK1 signaling for Kras oncogene-driven pancreatic cell plasticity and cancer. *Cancer Cell* **23,** 406–420 (2013).
27. Lesina, M. *et al.* Stat3/Socs3 activation by IL-6 transsignaling promotes progression of pancreatic intraepithelial neoplasia and development of pancreatic cancer. *Cancer Cell* **19,** 456–469 (2011).
28. Schönhuber, N. *et al.* A next-generation dual-recombinase system for time- and host-specific targeting of pancreatic cancer. *Nat. Med.* **20,** 1340–1347 (2014).
29. Prahallad, A. *et al.* Unresponsiveness of colon cancer to BRAF(V600E) inhibition through feedback activation of EGFR. *Nature* **483,** 100–103 (2012).
30. Corcoran, R. B. *et al.* EGFR-mediated re-activation of MAPK signaling contributes to insensitivity of BRAF mutant colorectal cancers to RAF inhibition with vemurafenib. *Cancer Discov.* **2,** 227–235 (2012).
31. Sun, C. *et al.* Intrinsic resistance to MEK inhibition in KRAS mutant lung and colon cancer through transcriptional induction of ERBB3. *Cell Rep.* **7,** 86–93 (2014).
32. Pettazzoni, P. *et al.* Genetic events that limit the efficacy of MEK and RTK inhibitor therapies in a mouse model of KRAS-driven pancreatic cancer. *Cancer Res.* **75,** 1091–1101 (2015).
33. Prahallad, A. *et al.* PTPN11 Is a Central Node in Intrinsic and Acquired Resistance to Targeted Cancer Drugs. *Cell Rep.* **12,** 1978–1985 (2015).
34. Manchado, E. *et al.* A combinatorial strategy for treating KRAS-mutant lung cancer. *Nature* **534,** 647–651 (2016).
35. Infante, J. R. *et al.* A randomised, double-blind, placebo-controlled trial of trametinib, an oral MEK inhibitor, in combination with gemcitabine for patients with untreated metastatic adenocarcinoma of the pancreas. *Eur. J. Cancer Oxf. Engl. 1990* **50,** 2072–2081 (2014).
36. Jänne, P. A. *et al.* Selumetinib Plus Docetaxel Compared With Docetaxel Alone and Progression-Free Survival in Patients With KRAS-Mutant Advanced Non-Small Cell Lung Cancer: The SELECT-1 Randomized Clinical Trial. *JAMA* **317,** 1844–1853 (2017).
37. Grosskopf, S. *et al.* Selective Inhibitors of the Protein Tyrosine Phosphatase SHP2 Block Cellular Motility and Growth of Cancer Cells in vitro and in vivo. *ChemMedChem* (2015). doi:10.1002/cmdc.201500015
38. Garcia Fortanet, J. *et al.* Allosteric Inhibition of SHP2: Identification of a Potent, Selective, and Orally Efficacious Phosphatase Inhibitor. *J. Med. Chem.* **59,** 7773–7782 (2016).
39. Alagesan, B. *et al.* Combined MEK and PI3K inhibition in a mouse model of pancreatic cancer. *Clin. Cancer Res. Off. J. Am. Assoc. Cancer Res.* **21,** 396–404 (2015).
40. Caunt, C. J., Sale, M. J., Smith, P. D. & Cook, S. J. MEK1 and MEK2 inhibitors and cancer therapy: the long and winding road. *Nat. Rev. Cancer* **15,** 577–592 (2015).
41. Mainardi, S. *et al.* PTPN11 is required for growth of KRAS mutant Non Small Cell Lung Cancer in vivo. *Nat. Med.* This issue.
42. Subramanian, A. *et al.* Gene set enrichment analysis: A knowledge-based approach for interpreting genome-wide expression profiles. *Proc. Natl. Acad. Sci.* **102,** 15545–15550 (2005).

Figure 1: Loss of *Ptpn11* profoundly inhibits KRAS^{G12D}-driven pancreatic and pulmonary carcinogenesis. (a) Representative H/E stained sections of pancreata from *Kras* (n=5) and *Kras;Ptpn11*$^{-/-}$ mice (n=6) at 36 weeks of age with similar results. Scale bars: 1000 µm. Insets: magnification x10. **(b)** mPanIN development (top) and relative intact, untransformed acinar area (bottom) in *Kras* and *Kras;Ptpn11*$^{-/-}$ pancreata. Lesions and acinar area were quantified over one whole H/E stained pancreatic section from mice with the indicated age (13 weeks *Kras*, 24 weeks *Kras;Ptpn11*$^{-/-}$: n=8 animals; 9, 24 weeks *Kras*: n=7 animals; 9, 13, 36 weeks *Kras;Ptpn11*$^{-/-}$: n=6 animals; 36 weeks *Kras*: n=5 animals). FOV: field of view. Mean with SEM. ***: p<0.001; **: p<0.01; unpaired two-tailed Student's *t*-test. **(c)** Kaplan-Meier analysis of tumor unrelated survival of *Kras* (n=32, median: 548d) and *Kras;Ptpn11*$^{-/-}$ (n=30, median: 685.5d) mice. Ticks indicate censored mice euthanized for decline in clinical condition, but without microscopic evidence of PDAC. Details for all mice of the *Kras;Ptpn11*$^{-/-}$ cohort are given in **Supplementary Fig. 3d**. Significance was determined by log-rank (Mantel-Cox) test. **(d)** Kaplan-Meier analysis of tumor free survival of *Kras;Ink4a/Arf*$^{-/-}$ (n=14, median: 58d) and *Kras;Ink4a/Arf*$^{-/-}$*;Ptpn11*$^{-/-}$ (n=19, median: undefined) mice. Ticks indicate censored mice euthanized due to paraparesis, without histological evidence of more than rare low grade PanIN in the pancreas (see **Supplementary Fig. 4d** for details). Significance was determined by log-rank (Mantel-Cox) test. **(e)** Kaplan-Meier analysis of tumor free survival of *Kras;Trp53*$^{-/-}$ (n=29, median: 69d) and *Kras;Trp53*$^{-/-}$*;Ptpn11*$^{-/-}$ (n=28, median=117d) mice. Ticks indicate censored mice euthanized due to decline in clinical condition, without histological evidence of PDAC (see **Supplementary Fig. 4c** for details). Significance was determined by log-rank (Mantel-Cox) test. **(f)** Lung adenocarcinoma model: *Ptf1a*$^{Cre-ex1}$ was replaced by transnasal inhalation of adenoviral Cre (AdCre). Representative H/E micrographs of lungs from *Kras;Trp53*$^{-/-}$ and *Kras;Trp53*$^{-/-}$*;Ptpn11*$^{-/-}$ mice 100 days after adenoviral Cre inhalation, illustrating difference in tumor development and tumor load; *Kras;Trp53*$^{-/-}$ (n=14) vs. *Kras;Trp53*$^{-/-}$*;Ptpn11*$^{-/-}$ (n=16) animals in the whole survival analysis cohorts with similar results, the mice shown here were chosen for demonstrative reasons given their equal survival time. Scale bars: 1000 µm. Insets: magnification x10.

Figure 2: Oncogenic KRAS depends on SHP2 for adequate activity during carcinogenesis. (a) Immunoblot with lysates from pancreatic tissue (9 week old mice) of *Kras* and *Kras;Ptpn11*$^{-/-}$ animals using the specific antibodies indicated. Three biologically independent samples per group are shown. HSP90 served as loading control. Full scan images are shown in **Supplementary Fig. 18a**. **(b)** RAF-RAS-binding-domain(RBD)-agarose affinity precipitation experiments of representative samples (two biologically independent

samples per group) from pancreatic tissue (13 week old mice) with *Kras* and *Kras;Ptpn11*$^{-/-}$ genotype. Pulldown of RAS-GTP was performed with commercially available RAF-RBD-agarose beads. Precipitates were immunoblotted using a pan-RAS- (labeled: pan-RAS-RAF-RBD) or a mutant KRAS^{G12D}-specific antibody (labeled: KRAS^{G12D}-RAF-RBD). Immunoblots of the input samples with the identical antibodies are displayed below (labeled: pan-RAS and KRAS^{G12D}, respectively). Numerical values indicate the ratio of densitometrically quantified signals from pulldown over input samples. Ratios are illustrated by the panels on the right. For uncropped images including molecular weight markers see **Supplementary Fig. 18b**. **(c,d)** Gene set enrichment analysis of mRNA microarray data from pancreatic tissue samples of 9 week old *Kras* and *Kras;Ptpn11*$^{-/-}$ mice (n=3 animals per group); analysis and statistics were performed using (GSEA) software provided by the Broad Institute, Cambridge, MA, USA, as previously described[42]. **(c)** The pie chart illustrates the fractions of highly significant enriched gene sets in the "Hallmark" collection in *Kras* (red) vs. *Kras;Ptpn11*$^{-/-}$ (blue) samples. The white pie piece represents non-significant gene sets. **(d)** Enrichment plots for KRAS signaling signatures from the "Hallmark" gene set collection: Left: One of the most significantly enriched gene sets in *Kras* samples (genes upregulated by KRAS signaling are enriched in *Kras*); Right: the unique enriched gene set in *Kras;Ptpn11*$^{-/-}$ samples (genes downregulated by KRAS signaling are enriched in *Kras;Ptpn11*$^{-/-}$*).* **(e)** Representative H/E micrographs of SHP2 proficient (*Ptpn11*$^{+/-}$) vs. deficient (*Ptpn11*$^{-/-}$) pancreatic epithelia at the indicated time points expressing constitutively active mutant PI3KCA (upper panel; *R26-LSL-Pik3ca*^{H1047R}*, Ptf1a*$^{Cre-ex1}$), or MEK1 (lower panel; *R26-LSL-Map2k1*$^{S218D/S222D}$*, Ptf1a*$^{Cre-ex1}$). Scale bars 100 µm. Quantification of ductal lesions (ADM + PanIN) was performed on one whole tissue section per mouse and is displayed as bar graphs on the right. 13, 24 weeks *Pik3ca;Ptpn11*$^{-/-}$ and 9 weeks *Map2k1;Ptpn11*$^{-/-}$: n=6 mice; 13, 24 weeks *Pik3ca;Ptpn11*$^{+/-}$, 13 weeks *Map2k1;Ptpn11*$^{-/-}$ and 9 weeks *Map2k1;Ptpn11*$^{+/-}$: n=5 mice; 13 weeks *Map2k1;Ptpn11*$^{+/-}$: n=4 mice. Mean with SD. Unpaired two-tailed Student's *t*-test.

Figure 3: Loss of SHP2 in established PDAC decelerates tumor progression and sensitizes to MEK inhibition. (a) Schematic of the experimental workflow with the dual recombinase PDAC model. Pancreatic tumors arise in *Pdx-Flpo*;*Kras*$^{FSF-G12D/+}$;*Trp53*$^{frt/frt}$;*R26*$^{FSF-CAG-CreERT2\ (positive\ or\ negative)}$;*Ptpn11*$^{fl/fl}$ mice, genetically engineered to allow a temporospatially controlled second recombination event through a tamoxifen-inducible Cre-recombinase, expressed only after Flpo-mediated recombination. Mice were monitored with MRI for tumor occurrence and received tamoxifen upon PDAC detection, leading to deletion of *Ptpn11* alleles in the epithelial tumor compartment of *FSF-CreRT*^{positive} mice. Mice without the *FSF-CreRT* allele served as controls. Tumor volume dynamics were continuously

followed with weekly MRI. **(b)** Representative MR-images of two exemplary mice taken at the indicated interval (inset; w: week) after tamoxifen-administration to mice with established PDAC (green outline). The top panel depicts sequential images of a mouse from the *FSF-CreRT*^{negative} control cohort (SHP2 proficient, blue outline; n=10 animals with similar results), the bottom panel of a mouse with loss of *Ptpn11* in the epithelial tumor compartment (SHP2 deficient, orange outline; n=8 animals with similar results). Scale bars: 1 cm. **(c)** Quantification of pancreatic volume change over time after tumor detection and tamoxifen administration as measured by MRI. *Ptpn11*$^{fl/fl}$ control cohort: n=10; *Ptpn11*$^{-/-}$ deletion cohort: n=8. Volume tracking curves for individual mice over the whole course of follow-up are available in **Supplementary Fig. 8c**. Mean with SD. *: p=0.04; paired two-tailed t-test. **(d,e)** *In vitro* deletion of *Ptpn11* with 4-OH-tamoxifen in a PDAC cell line derived from a *FSF-CreRT*^{positive} mouse; ethanol served as vehicle control: **(d)** Short-term proliferation (5d) of the resulting SHP2-proficient vs. -deficient cell line pair was quantified. One experiment with cells seeded as triplicates. Mean with SD. *: p=0.048; unpaired two-tailed t-test. **(e)** Loss of SHP2 was confirmed by immunoblot. Pulldown of RAS-GTP was performed with RAF-RBD-agarose beads. Precipitates and input samples were analyzed using the respective antibodies (labeling: see legend **Fig. 2b**). Numerical values indicate the ratio of densitometrically quantified signals from pulldown over input samples. β-actin represents the loading control. One experiment performed. Full scan images are shown in **Supplementary Fig. 18c**. **(f)** Colony formation assays with YAPC and PANC-1 *PTPN11* wild-type (wt) vs. knockout (ko) cells (two independent *PTPN11* knockout cell lines are shown), treated with MEK inhibitors selumetinib or trametinib at the indicated concentrations. Three independently repeated experiments with similar results. **(g)** Phospho-RTK Array with lysates from YAPC wild-type cells treated with selumetinib for 48h vs. untreated control (ctrl). RTKs with enhanced phosphorylation (antibodies are spotted in duplicate) in response to selumetinib are indicated with colored boxes. One experiment performed. **(h)** Immunoblot of lysates from YAPC wildtype and *PTPN11* knockout clone #1.1 and #2.12 cells treated with selumetinib for the indicated hours (h). HSP90 served as loading control. Three independently repeated experiments with similar results. Full scan images are shown in **Supplementary Fig. 18d**. For the corresponding analysis with PANC-1 cells see **Supplementary Fig. 10g**. **(i)** *In vitro* co-inhibition of MEK (selumetinib) and SHP2 (GS493 or SHP099) in colony formation experiments with YAPC and PANC-1 human pancreatic cancer cell lines. Three independently repeated experiments with similar results. For additional co-inhibition combinations and experiments with DAN-G see **Supplementary Fig. 11d**; for quantification and calculation of combination index scores see **Supplementary Fig. 11e,f**.

Figure 4: Dual MEK and SHP2 inhibition as a viable strategy to treat *KRAS* mutant tumors. (a) Representative MRI scan slices depicting PDAC tumor sections of *Kras;Trp53*$^{-/-}$ mice, treated with vehicle (n=8), GS493 (n=11), trametinib (n=11) or trametinib + GS493 (n=13), at the indicated time points (weeks) following the start of therapy (start ther), with similar results among the groups. Scale bars: 1 cm. **(b)** MRI tracking of individual *Kras;Trp53*$^{-/-}$ pancreatic volumes over the course of treatment. Number of mice as in (a). Note that trametinib and the combination therapy trametinib + GS493 were associated with morbidity necessitating euthanasia before occurrence of pancreatic volume relapse in a fraction of *Kras;Trp53*$^{-/-}$ animals; for details see figure legend **Supplementary Fig. 14b**. **(c)** Waterfall plot depicting individual relative total lesion volumes after four and six weeks of therapy in *Kras;Trp53*$^{-/-}$ AdCre NSCLC mice, treated with vehicle (n=5), GS493 (n=5), trametinib (n=6), or trametinib + GS493 (n=6). **(d)** Patient derived *ex vivo KRAS* mutant (ID_B25: KRAS^{G12V}) PDAC organoids treated with titrated trametinib, with or without three different concentrations of SHP099, for 6d. Representative dose-response curves, tabular listing of IC50s for trametinib with or without increasing concentrations of SHP099, and representative bright field micrographs of wells treated with DMSO control, trametinib 3 nM, and trametinib 3 nM + SHP099 5 µM are shown. Scale bars: 100 µm. Three independently repeated experiments with similar results. A second set of experiments with organoids established from a different PDAC is shown in **Supplementary Fig. 16**. **(e)** Macroscopic photographs after 28d of therapy, and tumor volume tracking of PDAC tissue xenograft ID_02 (KRAS^{G12D}), treated as indicated. Each trial-arm consisted of one mouse with two tumors implanted in the right and left flanks. The larger tumors are shown in the photographs and the volume-tracking plots. One experiment performed. For additional experiments with two different PDAC tissue xenografts see **Supplementary Fig. 17a**. **(f)** Immunoblots and RAF-RBD-agarose pulldowns of tissue lysates from PDAC ID_02 tissue xenograft tumors treated for 28d as indicated. Pulldown of RAS-GTP was achieved using RAF-RBD-agarose beads. Precipitates and input samples were analyzed using the respective antibodies (labeling: see legend **Fig. 2b**). β-actin served as loading control. One experiment performed. For uncropped images including molecular weight markers see **Supplementary Fig. 18e**.

ONLINE METHODS

Mouse strains. *Kras*$^{LSL\text{-}G12D/+}$ (Kras^{tm1Tyj})[18], *Ptf1a*$^{+/Cre\text{-}ex1}$ (Ptf1a$^{tm1(cre)Hnak}$)[43], *Ptpn11*$^{fl/fl}$ (Ptpn11^{tm1Gsf})[44], *Cdkn2a*$^{fl/fl}$ (Cdkn2a^{tm4Rdp})[20], *Trp53*$^{fl/fl}$ (Trp53^{tm1Brn})[45], *R26-LSL-Map2k1*$^{S218D/S222D}$ (Gt(ROSA)26Sor$^{tm8(Map2k1*,EGFP)Rsky}$)[25], *R26-LSL-Pik3ca*^{H1047R} (Gt(ROSA)26Sor$^{tm2(Pik3ca*)Das}$)[26], *Socs3*$^{fl/fl}$ (Socs3^{tm1Ayos})[46], *Kras*$^{FSF\text{-}G12D/+}$ (Kras^{tm1Dsa})[28], *Pdx-Flpo* (Tg(Pdx1-flpo)#Dsa)[28], *R26*$^{FSF\text{-}CAG\text{-}CreERT2}$ (Gt(ROSA)26Sor$^{tm3(CAG-Cre/ERT2)Dsa}$)[28], and *Trp53*$^{frt/frt}$ (Trp53$^{tm1.1Dgk}$)[47] have been described before. *R26*$^{td\text{-}EG}$ dual Flp/Cre reporter mice were generated by and obtained from D.S. Strains were interbred to obtain the following compound mutants: *Kras*$^{LSL\text{-}G12D/+}$, *Ptf1a*$^{Cre\text{-}ex1}$ (*Kras*); *Kras*$^{LSL\text{-}G12D/+}$, *Ptf1a*$^{Cre\text{-}ex1}$, *Ptpn11*$^{fl/fl}$ (*Kras;Ptpn11*$^{-/-}$); *Kras*$^{LSL\text{-}G12D/+}$, *Ptf1a*$^{Cre\text{-}ex1}$, *Cdkn2a*$^{fl/fl}$ (*Kras;Ink4a/Arf*$^{-/-}$); *Kras*$^{LSL\text{-}G12D/+}$, *Ptf1a*$^{Cre\text{-}ex1}$, *Cdkn2a*$^{fl/fl}$, *Ptpn11*$^{fl/fl}$ (*Kras;Ink4a/Arf*$^{-/-}$*;Ptpn11*$^{-/-}$); *Kras*$^{LSL\text{-}G12D/+}$, *Ptf1a*$^{Cre\text{-}ex1}$, *Trp53*$^{fl/+}$ (*Kras;Trp53*$^{+/-}$*);* *Kras*$^{LSL\text{-}G12D/+}$, *Ptf1a*$^{Cre\text{-}ex1}$, *Trp53*$^{fl/+}$, *Ptpn11*$^{fl/fl}$ (*Kras;Trp53*$^{+/-}$*;Ptpn11*$^{-/-}$*);* *Kras*$^{LSL\text{-}G12D/+}$, *Ptf1a*$^{Cre\text{-}ex1}$, *Trp53*$^{fl/fl}$ (*Kras;Trp53*$^{-/-}$*);* *Kras*$^{LSL\text{-}G12D/+}$, *Ptf1a*$^{Cre\text{-}ex1}$, *Trp53*$^{fl/fl}$, *Ptpn11*$^{fl/fl}$ (*Kras;Trp53*$^{-/-}$*;Ptpn11*$^{-/-}$*);* *R26-LSL-Map2k1*$^{S218D/S222D}$*,* *Ptf1a*$^{Cre\text{-}ex1}$, *Ptpn11*$^{fl/+}$ or *Ptpn11*$^{fl/fl}$ *(Map2k1;Ptpn11*$^{+/-}$ and *Map2k1;Ptpn11*$^{-/-}$*);* *R26-LSL-Pik3ca*^{H1047R}*,* *Ptf1a*$^{Cre\text{-}ex1}$, *Ptpn11*$^{fl/+}$ or *Ptpn11*$^{fl/fl}$ *(Pik3ca;Ptpn11*$^{+/-}$ and *Pik3ca;Ptpn11*$^{-/-}$*);* *Kras*$^{LSL\text{-}G12D/+}$, *Ptf1a*$^{Cre\text{-}ex1}$, *Socs3*$^{fl/fl}$, *Ptpn11*$^{fl/+}$ or *Ptpn11*$^{fl/fl}$ (*Kras;Socs3*$^{-/-}$*;Ptpn11*$^{+/-}$ and *Kras;Socs3*$^{-/-}$*;Ptpn11*$^{-/-}$*);* *Kras*$^{FSF\text{-}G12D/+}$, *Pdx-Flpo*, *Trp53*$^{frt/frt}$, *R26*$^{FSF\text{-}CAG\text{-}CreERT2\ positive\ or\ negative}$, *R26*$^{td\text{-}EG}$*,* *Ptpn11*$^{fl/fl}$ *(Kras;Trp53*$^{-/-}$*;FSF-CreRT*^{negative}*;Ptpn11*$^{fl/fl}$ and *Kras;Trp53*$^{-/-}$*;FSF-CreRT*^{positive}*;Ptpn11*$^{fl/fl}$*).* Mice with pancreatic deletion of *Ptpn11* by *Ptf1a*$^{Cre\text{-}ex1}$ were born at the expected Mendelian frequency and did not show any signs of impaired health, even with progressing age (data not shown). For mice of the lung tumor cohorts, nomenclature corresponds to those used for PDAC mice, yet for NSCLC mice, *Ptf1a*$^{Cre\text{-}ex1}$ was replaced by inhalation of Cre-expressing adenovirus (AdCre). All mice were kept in a mixed genetic background. Genotypes were determined by PCR and gel electrophoresis at weaning and after death. NSG mice were obtained from Jackson Laboratory and bred under a MTA with Klinikum rechts der Isar, Technische Universität München. All animal experiments and care were in accordance with the guidelines of institutional committees and approved by the local authority, Regierung von Oberbayern.

Inflammation-triggered accelerated pancreatic carcinogenesis. Chronic pancreatitis was induced by repetitive supramaximal stimulation with the cholecystokinin analogue caerulein (Sigma-Aldrich). Beginning at 8 weeks of age, *Kras* and *Kras;Ptpn11*$^{-/-}$ mice received 5 daily intraperitoneal high-dose injections of the secretagogue (200 µg/kg body weight) followed by 2 days of rest for a period of 4 consecutive weeks. Animals were euthanized and analyzed at 13 weeks of age (cf. schematic in **Supplementary Fig. 3e**).

Pancreatic epithelial explants: isolation and *in vitro* transdifferentiation assay. Pancreatic epithelial explants from 4 week old *Kras* and *Kras;Ptpn11*$^{-/-}$ mice were established by slightly modified previously published protocols[19,48]. In brief, the whole pancreas was collected and treated twice with 1.2 mg/ml collagenase from *Clostridium histolyticum* (Sigma-Aldrich). Following three wash steps with McCoy's 5A medium (Sigma-Aldrich) containing 0.2 mg/ml soybean trypsin inhibitor (Sigma-Aldrich) and 0.1% (wt/vol) BSA (Sigma-Aldrich), digested samples were filtered through a 100 µm cell strainer, resuspended in recovery medium (DMEM/F12 supplemented with 20% FBS and Penicillin-Streptomycin (100 U/ml, 100 µg/ml) (all: Life Technologies)) and allowed to recover for 1 hour at 37°C. Subsequently, cells were pelleted and either washed in ice-cold PBS and lysed for immunoblot-analyses or resuspended in culture medium, consisting of Waymouth's MB 752/1 (Life Technologies) supplemented with 0.2 mg/ml soybean trypsin inhibitor (Sigma-Aldrich), 50 µg/ml bovine pituitary extract (Life Technologies), insulin-transferrin-selenium (10 mg/ml, 5.5 mg/ml, 0.0067 mg/ml; Life Technologies), 0.1% FBS and Penicillin-Streptomycin. Rat tail collagen type I (Corning) at a final concentration of 2.5 mg/ml was added and the suspension was immediately plated into wells precoated with 2.5 mg/ml of rat tail collagen type I. After solidification, culture medium was placed on top of the gel. Explants were treated with indicated final concentrations of the SHP2 phosphatase inhibitor PHPS1 (Sigma-Aldrich) or vehicle control (DMSO) on day 1 and day 3 after plating. For quantification, acinar explants were seeded in triplicates. At day 5, all cell clusters were counted throughout whole wells and reported as percentage of duct-like spheres and acinar clusters.

Adenoviral Cre delivery and NSCLC model. Sporadic expression of Cre in mouse lungs was achieved by transnasal inhalation of engineered adenovirus (University of Iowa, Viral Vector Core) as previously described[49]. Following anesthesia with intraperitoneal medetomidine (0.5 mg/kg), midazolam (5 mg/kg) and fentanyl (0.05 mg/kg), a final volume of 60 µl MEM carrying $5*10^7$ plaque forming units of calcium phosphate co-precipitated Adeno-Cre was dispensed dropwise over the left nostril of 6-8 week old mice until inhaled in its entirety. Analgosedation was antagonized by subcutaneous atipamezole (2.5 mg/kg), flumazenil (0.5 mg/kg) and naloxone (1.2 mg/kg) and mice were monitored under a heat lamp in the biosafety hood until completely recovered.

Dual-recombinase system. Sequential genetic manipulation of the murine pancreas was accomplished through a combined Flpo-FRT and Cre-loxP system as previously reported[28]. Pancreatic tumors were initiated by *Pdx-Flpo* mediated recombination of *Kras*$^{FSF\text{-}G12D/+}$ and *Trp53*$^{frt/frt}$ alleles and expressed a tamoxifen-inducible Cre-recombinase from the R26-locus (*R26*$^{FSF\text{-}CAG\text{-}CreERT2}$). Mice were monitored by magnetic resonance imaging (MRI) as described

below and received 3 mg of tamoxifen (in 150 µl corn oil; Sigma-Aldrich) per oral gavage on three consecutive days when tumor volumes had reached 50-450 mm^3, resulting in excision of the floxed *Ptpn11* alleles. Mice lacking the $R26^{FSF\text{-}CAG\text{-}CreERT2}$ allele underwent the same procedure and served as controls. Dual recombination was confirmed by a double fluorescence/bioluminescence reporter allele ($R26^{td\text{-}EG}$), which upon Flpo-mediated recombination expresses EGFP and firefly luciferase, and after Cre-mediated recombination loses the EGFP/firefly sequences and expresses tdTomato and renilla luciferase.

For *in vitro* deletion of *Ptpn11* a primary *ex vivo* PDAC cell line was established from a moribund $Kras;Trp53^{-/-};FSF\text{-}CreRT^{positive};Ptpn11^{fl/fl}$ mouse and was treated daily with 2 µM 4-OH-tamoxifen (Sigma-Aldrich) or with vehicle control (pure ethanol) for six consecutive days. Loss of SHP2 was verified by immunoblotting.

Magnetic resonance imaging. MR-imaging experiments for $Kras;Trp53^{-/-}$, $Kras;Trp53^{-/-}$ Ad-Cre, and $Kras;Trp53^{-/-};FSF\text{-}CreRT^{negative};Ptpn11^{fl/fl}$ and $Kras;Trp53^{-/-};FSF\text{-}CreRT^{positive};Ptpn11^{fl/fl}$ mice were initiated at an age of 28-35 days and were repeated weekly as described previously[48]. Sedation was performed via continuous inhalation of 2% isoflurane (Abbott) in O_2 using a veterinary anesthesia system (Vetland Medical). Body temperature was maintained and monitored, eyes were protected by eye ointment. Image acquisition was achieved employing a microscopy surface coil inside a 3.0 tesla clinical device (Philips) and an axial multi-slice T2-weighted (T2w) TSE sequence (resolution 0.3 × 0.3 × 0.7 mm^3, 30 slices, TE = 90 ms, TR>3 s). Solid tumor volumes were calculated using OsiriX Lite DICOM viewer (Pixmeo) by summating truncated pyramid volumes between tumor areas on vicinal slices. On average, $Kras;Trp53^{-/-}$ mice at age 38 days (95% CI: 35 - 40 days) met inclusion criteria for the therapy trial with a mean pancreatic volume of 319 mm^3 (95% CI: 261 - 377 mm^3). $Kras;Trp53^{-/-}$ AdCre mice were enrolled for treatment at a mean time post-AdCre inhalation of 60 days (95% CI: 56 – 63 days) with a mean lesion load of 99 mm^3 (95% CI: 55 - 142 mm^3). Dosing and schedule of drug administration are detailed below.

Human PDAC specimens and patient-derived tissue xenografts. Pancreatic ductal adenocarcinoma tissues were obtained from patients who underwent surgical resection at the Koç University Hospital, Istanbul, Turkey (M.E.). All patients provided written informed consent. For the xenograft therapy trial samples (all $KRAS^{G12D}$) were procured and expanded *in vivo* under an MTA agreement at the Universidad Autónoma de Madrid and with approval of the ethical review board (CEI 60-1057-A068) and the Comunidad de Madrid (Red PROEX 335/14). Each sample was cut into approximately 200-300 mm^3 pieces. Fragments were coated in Matrigel basement membrane matrix (Corning) and implanted in subcutaneous

pockets in the posterior flanks of 8-week-old NSG mice. Tumors were passaged for two-three generations before initiation of treatment trials. Volumes were evaluated every 2-3 days by caliper measurements and the approximate volume (V) of the mass was estimated using the formula $V = D*d^2/2$ with D being the major tumor axis and d being the minor tumor axis. Established tumors (average volume at inclusion: 150-300 mm^3) were randomly assigned to trial arms and treated as specified below. Experiments were terminated once vehicle control tumors reached critical size at the ethical endpoint (V = 2000-4000 mm^3). End-of-treatment tumor material was snap-frozen in liquid nitrogen and stored at -80 °C for protein analysis.

Human pancreatic cancer cell line xenografts. Cells (numbers as indicated) were suspended in 100 µl of a 1:1 mixture of DMEM and Matrigel (Corning) and injected subcutaneously into the flanks of NSG mice. Tumor volume was monitored as indicated above for the tissue xenografts. Therapy was initiated after tumors had reached a volume of 50-100 mm^3. For drug dosing and schedule see below.

Drugs and inhibitors. Trametinib, selumetinib, pictilisib, oxaliplatin and paclitaxel were purchased from Selleckchem, gemcitabine was provided by the Hospital Pharmacy of Klinikum Rechts der Isar (Technische Universität München), and GS493 and SHP099 were synthesized and kindly provided by M.N., Medicinal Chemistry, Leibniz-Forschungsinstitut für Molekulare Pharmakologie, Berlin, Germany. PHPS1[50] was obtained from Sigma-Aldrich. Drugs were dissolved in DMSO to yield 5-50 mM stock solutions and stored at −80 °C.

***In vivo* therapy dosing.** For *in vivo* application in *Kras;Trp53*$^{-/-}$ and NSG mice, trametinib was diluted in 0.5% hydroxypropylmethylcellulose (Sigma-Aldrich) and 0.2% Tween-80 (Sigma-Aldrich) in water. GS493 was dissolved in Kolliphor EL (Sigma-Aldrich) and applied in an emulsion of 10% Kolliphor EL (Sigma-Aldrich), 10% ethanol and water. Trametinib (1 mg/kg) was administered by oral gavage (*Kras;Trp53*$^{-/-}$ mice: every other day; NSG mice: 5 days on, 2 days off) whereas GS493 was injected intraperitoneally (30 mg/kg, same schedule)[51].

Histology and Immunohistochemistry. Tissue specimens were either snap-frozen in OCT (Sakura Finetek) or fixed in 4% buffered paraformaldehyde, dehydrated and embedded in paraffin wax. 10 µm OCT cryo sections were used for lineage tracing fluorescence-microscopy after brief fixing in ethanol and nuclear staining with DAPI (Vector Laboratories). FFPE-sections of 3 µm were stained with hematoxylin/eosin (H/E), Sirius Red or used for immunohistochemical studies.

Immunohistochemistry was performed on murine and human FFPE-sections employing avidin-biotin enhancement (Vector Laboratories). The following antibodies were used: SHP2 (#3397; 1:200), pERK1/2 (#4376; 1:100), pSTAT3 Y705 (#9145; 1:100), pAKT (#3787; 1:50), Cleaved Caspase 3 (#9661; 1:200) from Cell Signaling, pSHP2 Y542 (ab62322; 1:500) and Ki67 (ab15580; 1:1000) from Abcam, Cyclin D1 (SP4; 1:100) from Thermo Scientific, and Amylase (#46657; 1:500) from Santa Cruz. Slides were developed with DAB (Vector Laboratories) and counterstained with hematoxylin. Image acquisition was achieved on a Zeiss AxioImager.A1 microscope. Quantitative analyses of tumor areas and IHC-staining were performed with Axiovision (Zeiss) and ImageJ softwares.

Cell Culture and cell lines. Primary murine tumor cell lines were established from chopped pieces of explanted tumors without enzymatic digestion. All murine cell lines were routinely cultured in Dulbecco's modified Eagle medium supplemented with 10% FBS and Penicillin-Streptomycin (100 U/ml, 100 µg/ml) (all Life Technologies). PANC-1 ($KRAS^{p.G12D}$; $P53^{p.R273H}$), YAPC ($KRAS^{p.G12V}$; $P53^{p.H179R}$; $SMAD4^{p.R515fs*22}$), DAN-G ($KRAS^{p.G12V}$; $P53^{p.GEYFTLQV325fs}$; $CDKN2A^{p.0}$), CAPAN-1 ($KRAS^{p.G12V}$; $P53^{p.A159V}$; $SMAD4^{p.S343*}$; $CDKN2A^{p.0}$), CAPAN-2 ($KRAS^{p.G12V}$; $TP53^{c.375G>T}$), ASPC-1 ($KRAS^{p.G12D}$; $P53^{p.C135fs*35}$; $SMAD4^{p.R100T}$; $CDKN2A^{p.L78fs*41}$), SU86.86 ($KRAS^{p.G12D}$; $P53^{p.G245S}$; $CDKN2A^{p.0}$), COLO357 ($KRAS^{p.G12D}$), T3M4 ($KRAS^{p.Q61H}$; $P53^{p.Y220C}$) and BXPC3 ($KRAS^{wt}$; $P53^{p.Y220C}$; $CDKN2A^{p.0}$; $SMAD4^{c.1\_1659del1659}$) were purchased from the Deutsche Sammlung von Mikroorganismen und Zellkulturen GmbH (DSMZ). H358 ($KRAS^{p.G12C}$), H2170 ($KRAS^{wt}$; $P53^{p.R158H}$; $CDKN2A^{p.0}$) and H1975 ($KRAS^{wt}$; $EGFR^{p.L858R/p.T790M}$; $PIK3CA^{p.G118D}$; $P53^{p.R273H}$; $CDKN2A^{p.E69*}$) were a kind gift from P. Jost (Klinikum rechts der Isar, Technische Universität München, Munich, Germany). Mutational status of the cell lines was compiled from ATCC (American Type Culture Collection), COSMIC (Catalogue of Somatic Mutations in Cancer, Wellcome Trust Sanger Institute) and CCLE (Cancer Cell line Encyclopedia, Broad Institue) databases. PANC-1 cells were cultured in DMEM, all other human cell lines in RPMI1640 (Life Technologies), supplemented with 10% FBS and Penicillin-Streptomycin (100 U/ml, 100 µg/ml). All cells were kept at 37°C in a humidified incubator with 5% CO_2.

Plasmids, Cloning and Transfection. To generate CRISPR/Cas9 *PTPN11* constructs, the pX458 vector was used to clone in gRNAs targeting the *PTPN11* gene. The oligonucleotide sequences for both *PTPN11* gRNAs are as follows: *PTPN11* gRNA 1: Fw: CACCGGAGGAACATGACATCGCGG, Rev: AAACCCGCGATGTCATGTTCCTCC; *PTPN11* gRNA 2: Fw: CCACGAACATGACATCGCGGAGGTG, Rev: AAACCACCTCCGCGATGTCATGTTC. Forward and reverse oligos for each gRNA were annealed and ligated into Bbs1 digested pX458 vector. Target cells were subsequently

transfected with the pX458-*PTPN11*-gRNA plasmids using polyethylenimine (PEI). Positively transfected cells expressing GFP were then FACS-sorted as single cells in 96-well plates. Clones were allowed to grow out and analyzed for SHP2 status. SHP2 knockout clones were then named after gRNA and clone name, e.g. YAPC #1.1 = gRNA1, clone 1.

$SHP2^{WT}$ and $SHP2^{C459S}$ reconstitution experiments: pCMV-GFP plasmid was available in the Birchmeier lab, pCMV-SHP2-WT (#8381) and pCMV-SHP2-C459S (#8382) plasmids were purchased from AddGene. SHP2 knockout clones were transfected with pCMV-GFP, pCMV-SHP2-WT or pCMV-SHP2-C459S using PEI. Subsequently, transfected cells were selected with G418 (800 µg/ml G418 until non-transfected control cells were dead, then maintained in 200 µg/ml G418) and clones that formed were picked and analyzed for SHP2 expression.

$SHP2^{E76A}$ reconstitution experiment: pBp-SHP2-E76A was purchased from Addgene (#8331); control vector pBp-GFP was available in the Birchmeier lab. Using PEI, the plasmids were transfected in AmphoPack-293 cells (Takara, cat. #631505) to produce amphotrophic viral particles. The virus-containing supernatant was subsequently used to transduce PANC-1 *PTPN11* knockout #2.6 cells in three consecutive rounds of infection. The viral supernatant was supplemented with 8 µg/ml polybrene. Infected cells were then selected in 2 µg/ml puromycin.

Phosphatase assay. To measure SHP2 phosphatase activity, sub-confluent cell lines (YAPC and PANC-1) were serum-starved (0.1% FBS) for 18 hours and then treated with selumetinib (or left untreated) in full growth medium (10% FBS) for 24 hours. Cells were then washed once with cold PBS and lysed on ice in cold PTP lysis buffer (25 mM Hepes, pH 7.4, 150 mM NaCl, 1 mM DTT, 2 mM EDTA, 0.5% Triton X-100, 1:50 diluted protease inhibitor cocktail (Serva)). Cell lysate supernatants (2 mg/each) were pre-cleared with Pierce™ protein A/G agarose (Life Technologies) for 1 hour, transferred to a new tube and incubated with SHP2 antibody (#3397, Cell Signaling) or a rabbit IgG control (Santa Cruz) at 4 °C on a rotator. Protein A/G agarose beads (60 µl/each, 50 % slurry) were added for additional 2 hours. Following a brief centrifugation, supernatants were collected for immunoblot analysis of IP efficiency. Immunoprecipitates were washed twice with PTP lysis buffer, twice with Reaction Buffer (25 mM Hepes, pH 7.4, 50 mM NaCl, 1 mM DTT, 0.05% Triton X-100), followed by resuspension in 100 µl reaction buffer containing 50 µM DiFMUP (Biomol) and incubated at room temperature for 20 min. After a brief centrifugation, supernatants were transferred into a 96-well plate and DIFMU (dephosphorylated DiFMUP) fluorescence signal was measured at 358 nm excitation and 455nm emission on a FLUOstar OPTIMA plate reader. The remaining immune complexes were used for immunoblotting analysis of SHP2 protein.

734 **Proliferation assays.** Cells were seeded in triplicate into 6-well plates and trypsinized,
735 collected and counted using trypan blue and Countess Automated Cell Counter (Invitrogen)
736 at indicated time points.
737
738 ***In vitro* drug screening and colony formation assays.** Cells were seeded into 6-, 12- or
739 24-well plates ($20x10^3$, $5x10^3$ or $1\text{-}4x10^3$ cells per well, respectively) and allowed to adhere
740 overnight in regular growth media. Cells were cultured in absence or presence of drugs as
741 indicated and refreshed every 2-3 days until the end of the experiment (in average after 10-
742 14 days). For each independent experiment, the different conditions were simultaneously
743 fixed in 3.5% formaldehyde or 6% glutaraldehyde and subsequently stained with 0.1% crystal
744 violet and digitalized on an image scanner. Relative growth was quantified by densitometry.
745 All experiments were performed at least twice and representative results are shown.
746
747 **Quantitative analysis of drug synergy.** Drug synergy was calculated using CompuSyn
748 software (version 1.0) which is based on the median-effect principle and the combination
749 index–isobologram theorem[52]. CompuSyn software generates combination index (CI) values,
750 where CI < 0.75 indicates synergism, CI = 0.75–1.25 indicates additive effects, and CI > 1.25
751 indicates antagonism. Following the instruction of the software, drug combinations at non-
752 constant ratios were used to calculate the combination index in our study.
753
754 **Patient-derived *ex vivo* PDAC organoid culture, treatment and read-out.** *Ex vivo*
755 organoids from resected human PDAC samples were generated and expanded as described
756 previously[53], with minor adaptations. In order to achieve conditions for high-throughput drug
757 screening, single cells were isolated from established organoids by enzymatic digestion and
758 gentle mechanical force. Cell-Matrigel suspensions were delivered into 96-well plates ($1x10^3$
759 cells/well) and single cells readily reformed organoids upon replating. After 24 hours, titration
760 treatments were initiated and cell viability was measured 5 days after drug addition via
761 CellTiter-Glo 3D Viability Assay (Promega) luminescence on a FLUOstar OPTIMA microplate
762 reader (BMG Labtech). All donors provided written informed consent and experiments were
763 approved by the local ethics committee of Faculty of Medicine, Technische Universität
764 München, Projects 1946/07 and 207/15.
765
766 **Western blotting, RAS-RAF-RBD pulldown, Phospho-Arrays.** Tissues were immediately
767 snap-frozen in liquid nitrogen at time of organ harvest. Tissues or cells were lysed in Mg^{2+}
768 lysis buffer (125 mM HEPES, pH 7.5, 750 mM NaCl, 5% Igepal CA-630, 50 mM MgCl2, 5
769 mM EDTA and 10% glycerol; Millipore) or in RIPA buffer (50 mM Tris pH7.4, 150 mM NaCl,
770 1% NP40, 0.1% SDS and 0.5% Sodiumdeoxycholate) supplemented with protease inhibitor

(Serva or Roche) and phosphatase inhibitor cocktails (Serva or Sigma-Aldrich). Protein concentrations were determined by Bradford assay (Bio-Rad). For western blotting, proteins were separated by SDS-PAGE in Laemmli buffer, transferred to nitrocellulose or PVDF membranes, and detected with the following antibodies: ERK1/2 (#9102 or sc-93/sc-154) and SHP2 (#3397 or sc-280) were from Cell Signaling or Santa Cruz. AKT (#9272), pAKT S473 (#9271), Cleaved Caspase 3 (#9661), IGFRβ (#3027), pIGFRβ Y1135/1136 (#3024), MET (#8198), pMET Y1234/1235 (#3126), RAS^{G12D} mutant specific (#14429), STAT3 (#9139), and pSTAT3 Y705 (#9131) were purchased from Cell Signaling. HSP90 (sc-7947) and PCNA (sc-56) were from Santa Cruz, pSHP2 Y542 (ab51174) and KRAS (ab180772) were from Abcam. pan-RAS (05-516) was acquired from Millipore and β-actin-HRP (A3854) from Sigma-Aldrich. Signal detection was performed using horseradish peroxidase-conjugated secondary antibodies and ECL reagent (Amersham, GE Healthcare) followed by signal read-out in a Fusion SL-3 imaging system (Vilber) or by development on film. Ras-GTP levels were measured using the Ras Activation Assay Kit from Millipore (17-218) per manufacturer's instructions. Briefly, fresh pancreatic tissue or PDAC cell lines were lysed in ice-cold Mg^{2+} lysis buffer and equal amounts of protein were incubated with RAF-1-RBD agarose beads for 45 min at 4°C on a rotator. After three washing steps, beads were suspended in Laemmli reducing sample buffer, subjected to SDS-PAGE and blotted on nitrocellulose membranes. Detection was performed with the indicated antibodies. The human Phospho-Kinase and Phospho-RTK Arrays were purchased from R&D Systems (ARY003B and ARY001B) and were used according to the provided protocols. As the Phospho-Kinase Array is validated only for human samples, probable crossreaction of most of the spotted antibodies with corresponding murine antigens was confirmed by the manufacturer. Densitometric quantification of immunoblots or Phospho-Arrays was performed with ImageJ software.

Publicly available transcriptomics databases. Comparative transcriptomic analyses between normal pancreas and pancreatic cancer were performed integrating all available datasets on the oncogenomic web-portal Oncomine™. Correlation of *PTPN11* expression with patient survival in pancreatic adenocarcinoma and *KRAS* mutant lung adenocarcinoma was analyzed in 'The Cancer Genome Atlas (TCGA)' RNAseq PAAD and LUAD datasets, accessible via the University of California Santa Cruz (UCSC), Xena public data hub.

Microarray data analysis. Fresh pancreatic tissue samples from 9 week old *Kras* and *Kras;Ptpn11*$^{-/-}$ mice were homogenized and lysed in RLT lysis buffer (Qiagen) supplemented with 1:100 2-mercaptoethanol (Sigma-Aldrich). Sample processing and Affymetrix microarray hybridization (GeneChip (Mus musculus) Mouse Gene 1.0 ST arrays) were carried out at a

genomics core facility: Center of Excellence for Fluorescent Bioanalytics (KFB, University of Regensburg, Germany). Gene expression microarray data were analyzed using gene set enrichment analysis (GSEA) software provided by the Broad Institute, Cambridge, MA, USA, as previously described[42]. A false discovery rate (FDR q-value) of less than 0.25 and a nominal p-value of less than 0.05 were considered statistically significant.

Statistical analysis. Kaplan-Meier survival curves were calculated from all individual survival times of mice from the different genotype cohorts. Curves were compared by log-rank (Mantel-Cox) test to detect significant differences between the groups. For image quantifications and cell proliferation assays, statistical significance was assayed by unpaired two-tailed Student's t-test or Mann-Whitney test for comparison of two groups and by one-way ANOVA with post-hoc Tukey's test for more than two groups (variances were first examined by *F*-test or Brown-Forsythe test, respectively); ***: $P < 0.001$; **: $P < 0.01$; *: $P < 0.05$. Statistical analysis was performed with GraphPad PRISM® 7.0 software. Data are represented as dot plots with bar graphs for mean and standard deviation (SD) or standard error of the mean (SEM) as indicated, or as box-and-whisker plots with boxes ranging from 25th to 75th percentile, whiskers from minimum to maximum and the median as centre.

Data availability statement. Microarray hybridization raw data used for gene set enrichment analyses (represented in **Fig. 2** and **Supplementary Fig. 6)** were deposited in the EMBL-EBI ArrayExpress database under accession number E-MTAB-6399.

Also see the attached **Life Sciences Reporting Summary** for information on experimental design and reagents.

REFERENCES (ONLINE METHODS)

43. Nakhai, H. *et al.* Ptf1a is essential for the differentiation of GABAergic and glycinergic amacrine cells and horizontal cells in the mouse retina. *Development* **134,** 1151–1160 (2007).
44. Zhang, E. E., Chapeau, E., Hagihara, K. & Feng, G.-S. Neuronal Shp2 tyrosine phosphatase controls energy balance and metabolism. *Proc. Natl. Acad. Sci. U. S. A.* **101,** 16064–16069 (2004).
45. Marino, S., Vooijs, M., van Der Gulden, H., Jonkers, J. & Berns, A. Induction of medulloblastomas in p53-null mutant mice by somatic inactivation of Rb in the external granular layer cells of the cerebellum. *Genes Dev.* **14,** 994–1004 (2000).
46. Yasukawa, H. *et al.* IL-6 induces an anti-inflammatory response in the absence of SOCS3 in macrophages. *Nat. Immunol.* **4,** 551–556 (2003).
47. Lee, C.-L. *et al.* Generation of primary tumors with Flp recombinase in FRT-flanked p53 mice. *Dis. Model. Mech.* **5,** 397–402 (2012).
48. Mazur, P. K. *et al.* Combined inhibition of BET family proteins and histone deacetylases as a potential epigenetics-based therapy for pancreatic ductal adenocarcinoma. *Nat. Med.* **21,** 1163–1171 (2015).
49. DuPage, M., Dooley, A. L. & Jacks, T. Conditional mouse lung cancer models using

851 adenoviral or lentiviral delivery of Cre recombinase. *Nat. Protoc.* **4,** 1064–1072 (2009).
852 50. Hellmuth, K. *et al.* Specific inhibitors of the protein tyrosine phosphatase Shp2
853 identified by high-throughput docking. *Proc. Natl. Acad. Sci. U. S. A.* **105,** 7275–7280 (2008).
854 51. Lan, L. *et al.* Shp2 signaling suppresses senescence in PyMT-induced mammary
855 gland cancer in mice. *EMBO J.* (2015). doi:10.15252/embj.201489004
856 52. Chou, T.-C. Drug combination studies and their synergy quantification using the
857 Chou-Talalay method. *Cancer Res.* **70,** 440–446 (2010).
858 53. Boj, S. F. *et al.* Organoid models of human and mouse ductal pancreatic cancer. *Cell*
859 **160,** 324–338 (2015).

Figure1

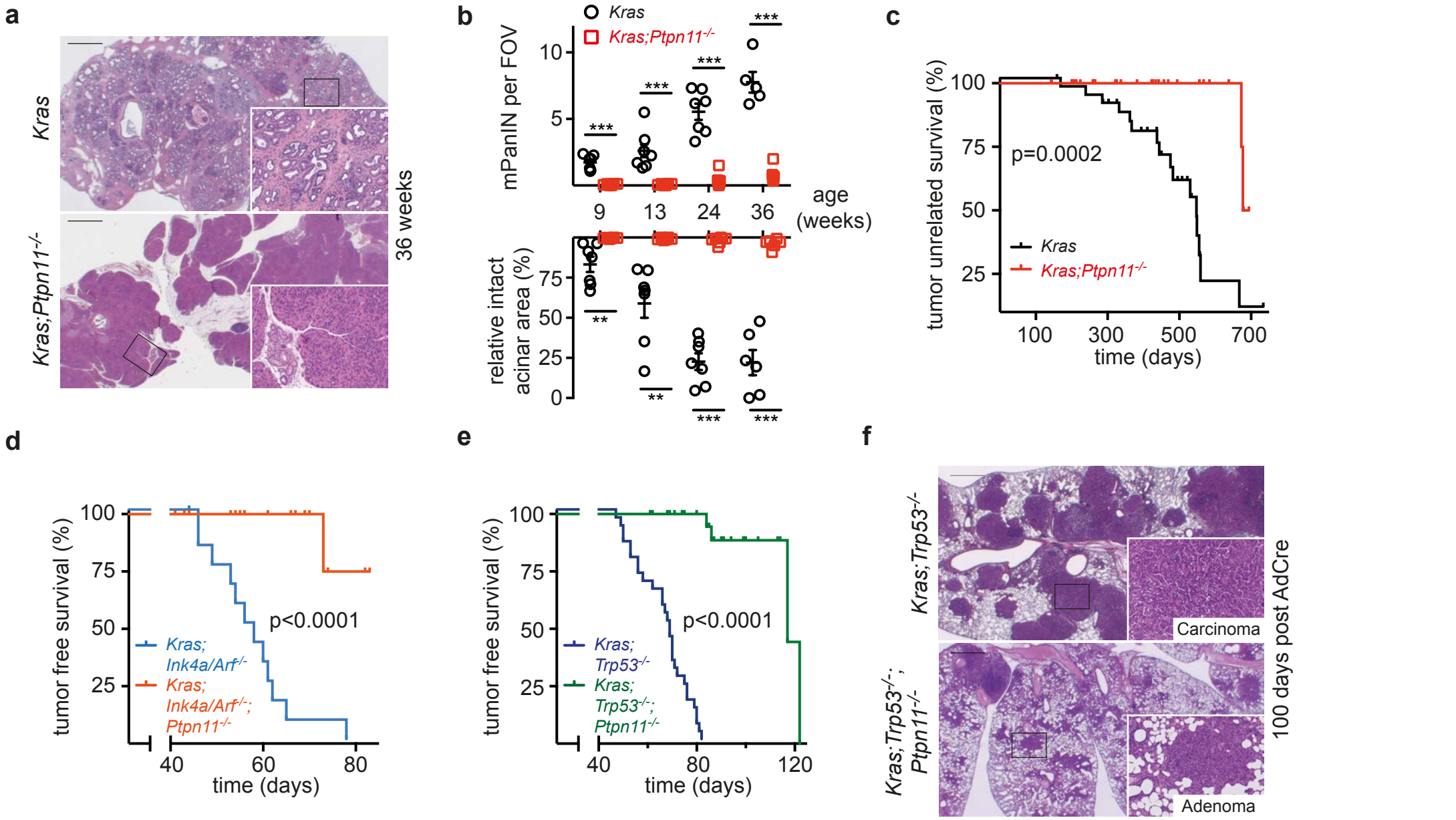
a
Kras
Kras;Ptpn11-/-
36 weeks
b
Kras
Kras;Ptpn11-/-
mPanIN per FOV
10
5
***
***
***
***
9
13
24
36
age (weeks)
relative intact acinar area (%)
75
50
25
0
**
**
***
***
c
tumor unrelated survival (%)
100
75
50
25
p=0.0002
Kras
Kras;Ptpn11-/-
100
300
500
700
time (days)
d
tumor free survival (%)
100
75
50
25
p<0.0001
Kras; Ink4a/Arf-/-
Kras; Ink4a/Arf-/-; Ptpn11-/-
40
60
80
time (days)
e
tumor free survival (%)
100
75
50
25
p<0.0001
Kras; Trp53-/-
Kras; Trp53-/-; Ptpn11-/-
40
80
120
time (days)
f
Kras;Trp53-/-
Kras;Trp53-/-; Ptpn11-/-
Carcinoma
Adenoma
100 days post AdCre

Figure2

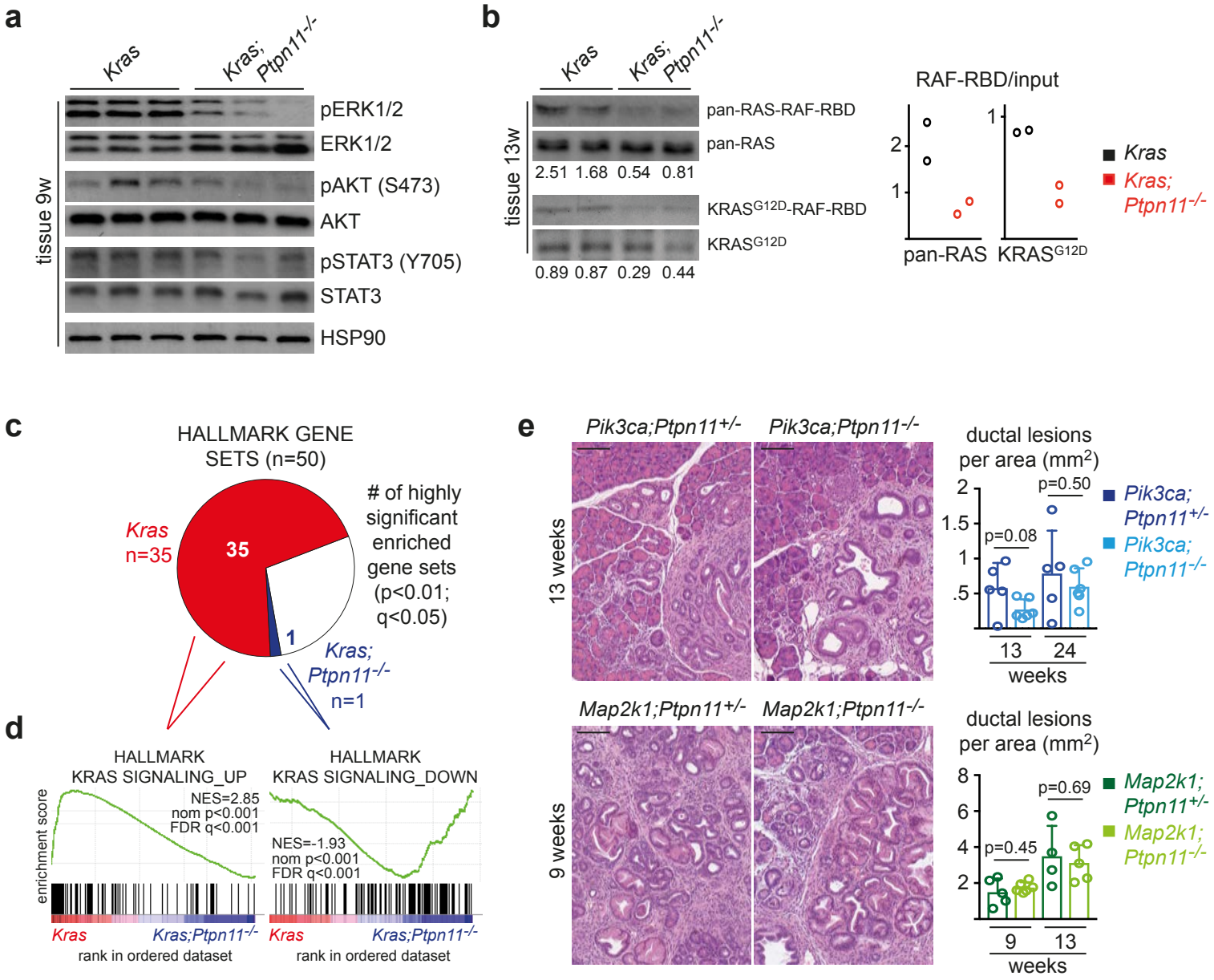
a
Kras
Kras; Ptpn11-/-
tissue 9w
pERK1/2
ERK1/2
pAKT (S473)
AKT
pSTAT3 (Y705)
STAT3
HSP90
b
Kras
Kras; Ptpn11-/-
tissue 13w
pan-RAS-RAF-RBD
pan-RAS
2.51 1.68 0.54 0.81
KRASG12D-RAF-RBD
KRASG12D
0.89 0.87 0.29 0.44
RAF-RBD/input
pan-RAS
KRASG12D
Kras
Kras; Ptpn11-/-
c
HALLMARK GENE SETS (n=50)
Kras n=35
35
1
Kras; Ptpn11-/- n=1
# of highly significant enriched gene sets (p<0.01; q<0.05)
d
HALLMARK KRAS SIGNALING_UP
NES=2.85
nom p<0.001
FDR q<0.001
HALLMARK KRAS SIGNALING_DOWN
NES=-1.93
nom p<0.001
FDR q<0.001
enrichment score
Kras
Kras;Ptpn11-/-
rank in ordered dataset
e
Pik3ca;Ptpn11+/-
Pik3ca;Ptpn11-/-
13 weeks
ductal lesions per area (mm2)
p=0.08
p=0.50
13
24
weeks
Pik3ca; Ptpn11+/-
Pik3ca; Ptpn11-/-
Map2k1;Ptpn11+/-
Map2k1;Ptpn11-/-
9 weeks
ductal lesions per area (mm2)
p=0.45
p=0.69
9
13
weeks
Map2k1; Ptpn11+/-
Map2k1; Ptpn11-/-

Figure3

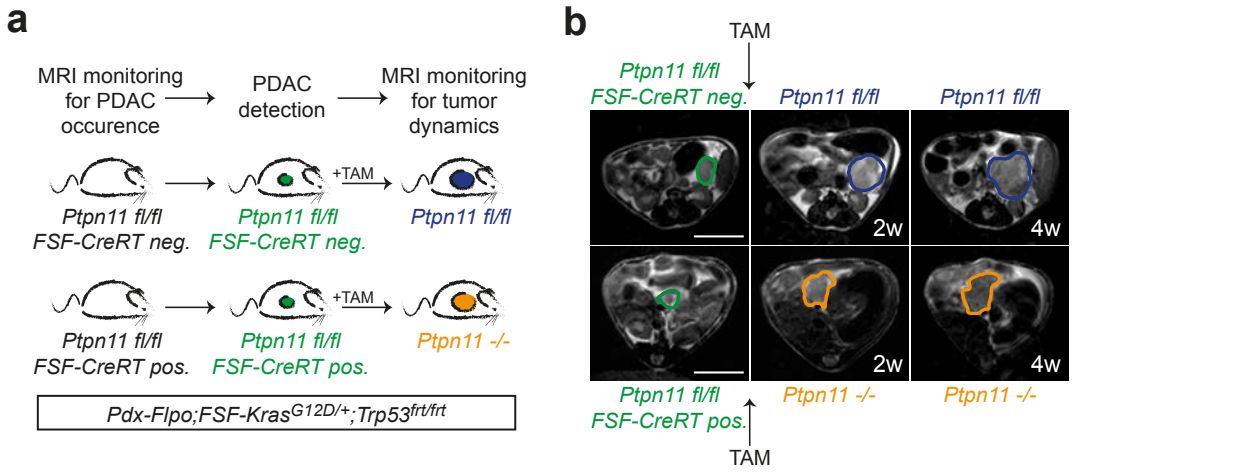
a
MRI monitoring for PDAC occurence
PDAC detection
MRI monitoring for tumor dynamics
+TAM
Ptpn11 fl/fl FSF-CreRT neg.
Ptpn11 fl/fl FSF-CreRT neg.
Ptpn11 fl/fl
Ptpn11 fl/fl FSF-CreRT pos.
Ptpn11 fl/fl FSF-CreRT pos.
Ptpn11 -/-
Pdx-Flpo;FSF-KrasG12D/+;Trp53frt/frt
b
TAM
Ptpn11 fl/fl FSF-CreRT neg.
Ptpn11 fl/fl
Ptpn11 fl/fl
2w
4w
2w
4w
Ptpn11 fl/fl FSF-CreRT pos.
Ptpn11 -/-
Ptpn11 -/-
TAM

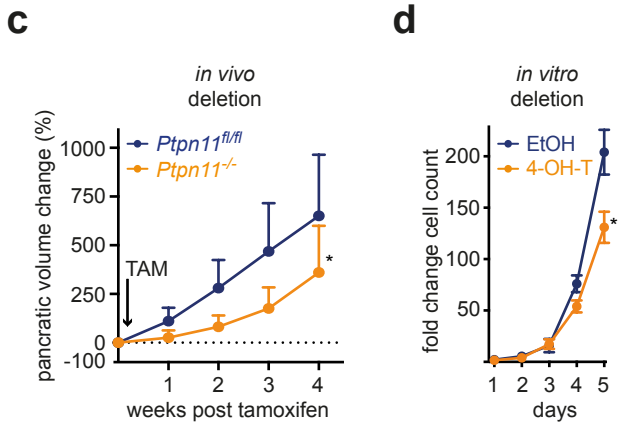
c
in vivo deletion
pancratic volume change (%)
Ptpn11fl/fl
Ptpn11-/-
TAM
weeks post tamoxifen

d
in vitro deletion
fold change cell count
EtOH
4-OH-T
days

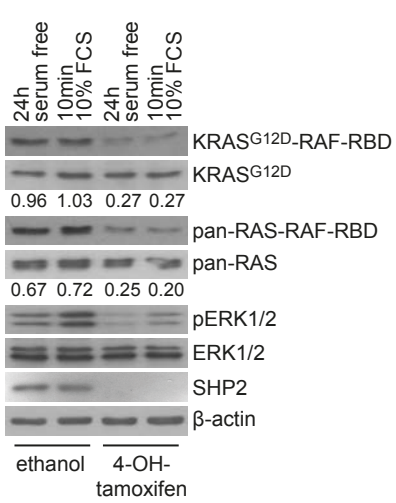
e
24h serum free
10min 10% FCS
KRASG12D-RAF-RBD
KRASG12D
0.96 1.03 0.27 0.27
pan-RAS-RAF-RBD
pan-RAS
0.67 0.72 0.25 0.20
pERK1/2
ERK1/2
SHP2
β-actin
ethanol
4-OH-tamoxifen

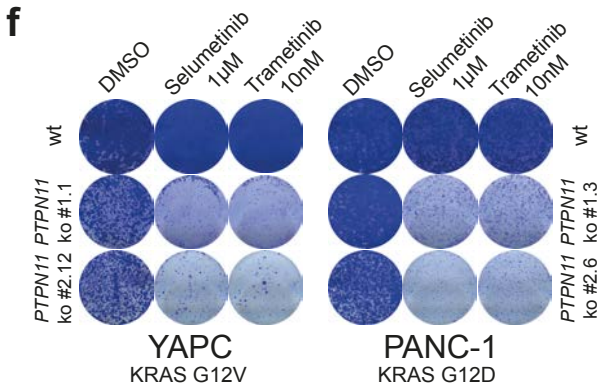
f
DMSO
Selumetinib 1μM
Trametinib 10nM
wt
PTPN11 ko #2.12
PTPN11 ko #1.1
PTPN11 ko #2.6
PTPN11 ko #1.3
YAPC
KRAS G12V
PANC-1
KRAS G12D

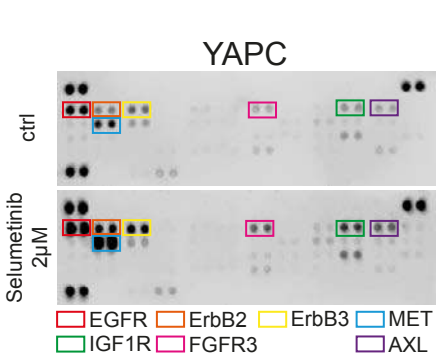
g
YAPC
ctrl
Selumetinib 2μM
EGFR
ErbB2
ErbB3
MET
IGF1R
FGFR3
AXL

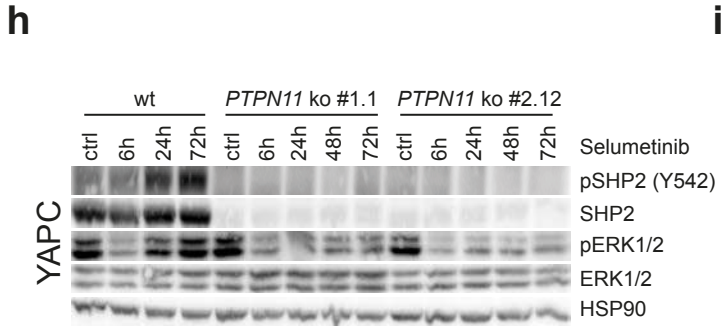
h
wt
PTPN11 ko #1.1
PTPN11 ko #2.12
ctrl
6h
24h
48h
72h
Selumetinib
pSHP2 (Y542)
SHP2
pERK1/2
ERK1/2
HSP90
YAPC

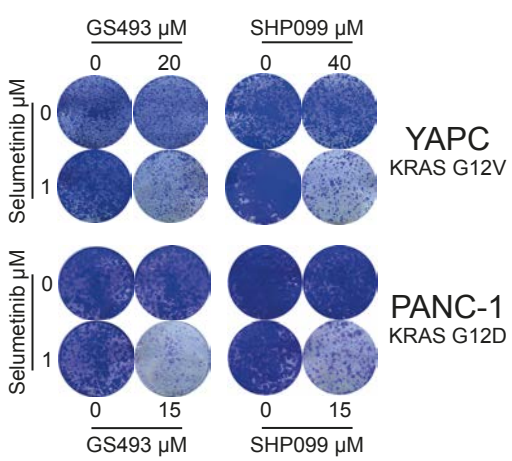
i
GS493 μM
SHP099 μM
0
20
40
Selumetinib μM
YAPC
KRAS G12V
PANC-1
KRAS G12D
15

Figure4

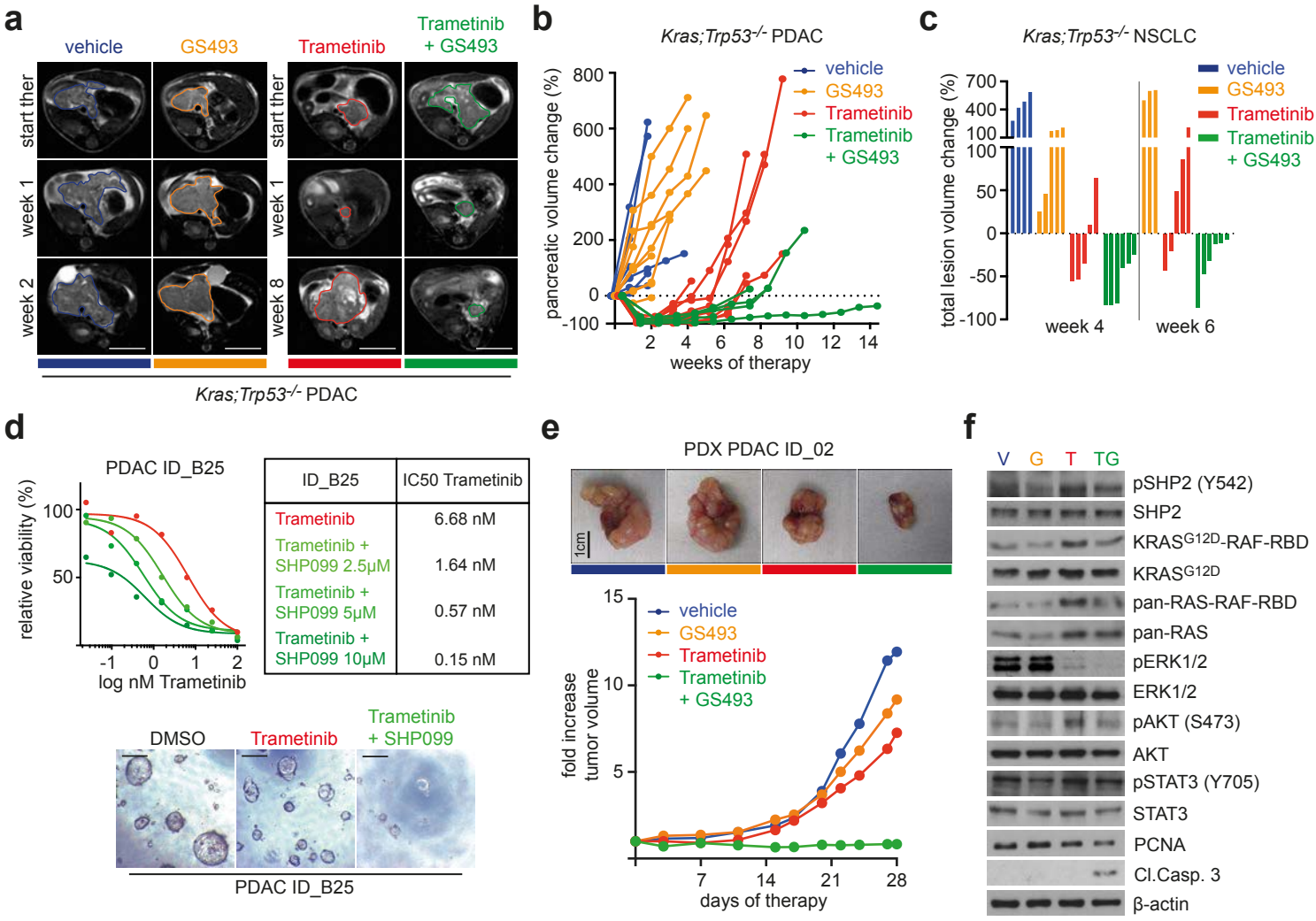
a
vehicle
GS493
Trametinib
Trametinib + GS493
start ther
week 1
week 2
week 8
Kras;Trp53-/- PDAC
b
Kras;Trp53-/- PDAC
pancreatic volume change (%)
weeks of therapy
vehicle
GS493
Trametinib
Trametinib + GS493
c
Kras;Trp53-/- NSCLC
total lesion volume change (%)
week 4
week 6
d
PDAC ID_B25
relative viability (%)
log nM Trametinib
ID_B25 | IC50 Trametinib
Trametinib | 6.68 nM
Trametinib + SHP099 2.5μM | 1.64 nM
Trametinib + SHP099 5μM | 0.57 nM
Trametinib + SHP099 10μM | 0.15 nM
DMSO
Trametinib
Trametinib + SHP099
PDAC ID_B25
e
PDX PDAC ID_02
1cm
fold increase tumor volume
days of therapy
f
V G T TG
pSHP2 (Y542)
SHP2
KRASG12D-RAF-RBD
KRASG12D
pan-RAS-RAF-RBD
pan-RAS
pERK1/2
ERK1/2
pAKT (S473)
AKT
pSTAT3 (Y705)
STAT3
PCNA
Cl.Casp. 3
β-actin